J. Fluid Mech. (1999), *vol.* 379, *pp.* 319–331. Printed in the United Kingdom

Mass-transfer enhancement via chaotic laminar flow within a droplet

By MICHELLE D. BRYDEN† AND HOWARD BRENNER

Department of Chemical Engineering, Massachusetts Institute of Technology, Cambridge, MA 02139-4307, USA

(Received 21 October 1996 and in revised form 31 July 1998)

The Stokes flow occurring within a non-neutrally buoyant spherical droplet translating by buoyancy through an immiscible liquid which is undergoing simple shear is shown to be chaotic under many circumstances for which the droplet translates by buoyancy through the entraining fluid. This flow is easily produced, for example, when the droplet rises (or falls) through the annular space of a vertical concentric-cylinder Couette viscometer or through a vertical Poiseuille flow. The parameters studied include: (i) droplet/bulk fluid viscosity ratio; (ii) shear strength/bubble rise velocity ratio; and (iii) the angle between the translational bubble velocity vector and the vorticity vector characterizing the undisturbed shear. Streamlines existing within a droplet that translates perpendicular to this vorticity vector are shown to be non-chaotic for all choices of physical parameters. Other relative orientations frequently contain chaotic trajectories. When solute initially dissolved within the droplet is extracted into the bulk fluid, the resulting overall mass-transfer coefficient (calculated via generalized Taylor dispersion theory) quantifying the extraction rate at asymptotically long times is shown to be significantly higher in the chaotic flow case.

1. Introduction

Much of the existing literature concerned with laminar chaos focuses on the local mixing properties of such flows (see Ottino 1990 for a review) and utilizes qualitative measures of the extent of chaotic motion, accompanied by visualization of the regions exhibiting chaotic behaviour in the form of Poincaré sections. Less common have been quantitative studies of the degree of global enhancement of the heat- and mass-transfer rates engendered by such chaotic laminar flows. Jana & Ottino (1992) studied heat transfer in a chaotic cavity flow. They considered the approach to equilibrium of an initially isothermal fluid that is perturbed by a step change in the wall temperature. Significant enhancement was found in the rate of heat transfer for circumstances in which chaotic transport was present. The net heat transfer rate displayed a strong dependence on the Péclet number (*Pe*), exhibiting a maximum at intermediate values of *Pe*. Ghosh, Chang & Sen (1992) investigated heat transfer in the annular space between rotating eccentric cylinders when the cylinders were maintained at a different temperatures. Although their work was limited to both small eccentricities and small oscillations superposed on an otherwise steady rotary flow – conditions under which chaotic transport would be expected to be small – they nevertheless found a significant increase in heat transfer occurring in circumstances where chaotic transport was present. Toussaint, Carrière & Raynal (1995) studied

† Present address: Westvaco Corp., 11101 Johns Hopkins Rd., Laurel, MD 20723, USA.

the rate of decay of an initially inhomogeneous scalar field in the presence of both chaotic and non-chaotic flows, demonstrating that the rate of decay to homogeneity was greater in the chaotic flow case.

Recently, Bryden & Brenner (1996) studied reaction and dispersion in time-periodic eccentric annular flow. They calculated the rate of disappearance of a solute which undergoes an instantaneous, irreversible chemical reaction on the surface of one of the alternately rotating cylinders, and found that the presence of chaotic laminar motion increases the effective reaction rate quantifying the resulting first-order macroscale kinetics beyond that occurring for comparable non-chaotic convection configurations. In addition, the presence of laminar chaos was shown to cause the effective axial solute/solvent velocity ratio to approach the perfectly-mixed value of unity in contrast with the corresponding non-chaotic annular flow case. The improved transverse mixing resulting from the chaotic motion also reduced the axial Taylor dispersivity dramatically.

Many other practical applications of laminar chaos in transport processes remain to be investigated. This paper addresses one such application, namely the extraction of a solute from a non-neutrally-buoyant dispersed phase into an entraining bulk fluid undergoing shear. Chaotic flows within spherical drops have been studied by Bajer & Moffatt (1990) as well as by Stone, Nadim & Strogatz (1991), the former considering a general quadratic flow within a sphere and the later studying the behaviour of the streamlines immersed within a general linear flow. Another three-dimensional confined flow exhibiting chaotic behaviour is the time-dependent spherical Couette flow considered by Cartwright, Feingold & Piro (1996). The work of Stone *et al.* (1991) is the most relevant in the context of our work. They demonstrated that the particle paths within a drop immersed in a general linear Stokes flow may wander chaotically, with the extent of chaotic motion depending upon the orientation of the vorticity vector relative to the principal axes of strain of the shear flow as well as upon the relative magnitudes of the vorticity and shear rate. However, they did not consider circumstances in which the drop translates relative to the bulk fluid, which their preliminary results suggested exhibited behaviour similar to that observed for their stationary drop case. In addition, they noted that the pathlines arising for the simple shear flow case are non-chaotic.

In the present contribution we focus on the superposition of the two above-mentioned flows, whereby a spherical drop translates through a simple shear flow. In combination, these elementary flows display chaotic behaviour. The structure of the resulting Poincaré sections differs appreciably from those observed in the flows considered by Stone *et al.* (1991). Potential fundamental and practical interest centres on the flows considered herein, owing to the ease with which they can be realized experimentally, in addition to their applicability to common chemical engineering processes such as liquid–liquid extraction. Poincaré sections for these flows are presented in §3 and the parameter range established for which chaotic flows occur. Section 4 presents the values of the overall mass-transfer coefficient, both for circumstances in which the flow internal to the drop is chaotic as well as when it is non-chaotic, thereby providing a quantitative global measure of the chaotically-enhanced improvement in extraction rate.

2. The flow field internal to the drop

The circumstance to be considered is that of a spherical droplet translating by buoyancy through a fluid undergoing a simple shear flow. Different angles α between

the direction of the vorticity vector $\boldsymbol{\omega}$ of the undisturbed shear flow and the direction of the gravity vector $\boldsymbol{g}$ will be investigated, with particular attention paid to the limiting cases in which $\boldsymbol{\omega}$ is either parallel ($\alpha = 0$) or perpendicular ($\alpha = \frac{1}{2}\pi$) to gravity. Each of these configurations is easily produced: the former results from allowing the bubble to rise or fall through the annular space between two vertical concentric cylinders, wherein a Couette flow is maintained by their relative rotation; the latter results when a bubble rises or falls within a Poiseuille flow occurring in a vertical tube. (For definiteness in the subsequent analysis, the relative translational motion of the droplet will always be described as if it were rising through the fluid, i.e. moving opposite to the direction of gravity.) Intermediate angle flows ($0 < \alpha < \frac{1}{2}\pi$) are also easily realized by combining the circular Couette flow with an annular Poiseuille flow. As will be seen later, the two limiting angles yield flows which display strikingly different behaviour, with the $\alpha = 0$ case containing large regions in which the particle paths within the droplet are chaotic, whereas the $\alpha = \frac{1}{2}\pi$ case contains only periodic pathlines. In circumstances where the externally-imposed flow is not strictly a *linear* shear flow it may nevertheless be regarded as such in proximity to the droplet, provided that the droplet radius a is small compared with both the characteristic linear dimension of the apparatus in which the external flow is generated and the distance of the droplet from the walls of this apparatus. The droplet will be assumed to remain spherical, a condition which requires *inter alia* that the respective Reynolds numbers based on translation and shear both be small compared to unity, and that the interface be inviscid (i.e. devoid of any special interfacial rheological properties (Edwards, Brenner & Wasan 1991) other than interfacial tension). Accordingly, in the quasi-steady Stokes flow case the complete flow occurring within the droplet is simply the linear superposition of the respective flows resulting from the bubble's translation through the quiescent fluid and from the external shear flow for the neutrally- buoyant droplet case.

The internal flow created by the bubble's translation is an axisymmetric Stokes flow of the form (Hadamard 1911)

$$\boldsymbol{v}_T = \frac{1}{2a^2(1+\sigma)}\boldsymbol{U}\cdot[\boldsymbol{x}x - (2r^2 - a^2)\boldsymbol{I}], \tag{2.1}$$

in which $\sigma = \mu_i/\mu_o$ is the droplet/external-fluid viscosity ratio, $\boldsymbol{x}$ is the position vector measured from the centre of the drop, $r^2 = \boldsymbol{x}\cdot\boldsymbol{x}$, and

$$\boldsymbol{U} = \frac{2a^2\Delta\rho g}{9\mu_o}\frac{1+\sigma}{\frac{2}{3}+\sigma}\hat{\boldsymbol{g}} \tag{2.2}$$

is the bubble velocity, with $\Delta\rho$ the algebraically-signed droplet/external-fluid density difference, $g = |\boldsymbol{g}|$ the acceleration due to gravity, $\hat{\boldsymbol{g}} \equiv \boldsymbol{g}/g$ a unit vector parallel to gravity, and a the droplet radius. Typical streamlines resulting from this flow are plotted in figure 1.

A general external shear flow of the form $\boldsymbol{v}^\infty = \boldsymbol{x}\cdot\boldsymbol{G}$, with $\boldsymbol{G} \equiv \nabla\boldsymbol{v}^\infty$ the undisturbed velocity gradient, induces a fully three-dimensional flow within the droplet. The internal flow field for a neutrally-buoyant droplet possessing an inviscid interface and suspended within such a shear flow is given by Taylor (1932) as

$$\boldsymbol{v}_G = \frac{1}{4a^2(1+\sigma)}[(5r^2 - 3a^2)(\boldsymbol{G} + \boldsymbol{G}^\dagger)\cdot\boldsymbol{x} - 2\boldsymbol{x}\boldsymbol{x}\cdot\boldsymbol{G}\cdot\boldsymbol{x}] + \tfrac{1}{2}\boldsymbol{\omega}\times\boldsymbol{x}, \tag{2.3}$$

with $\boldsymbol{\omega} = \nabla\times\boldsymbol{v}^\infty$ the vorticity vector. For the simple shear flow $\boldsymbol{v}^\infty = \boldsymbol{i}_2 G x_1$, we

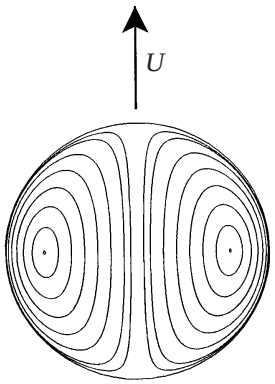

FIGURE 1. Streamlines internal to a spherical droplet rising by buoyancy through a quiescent fluid.

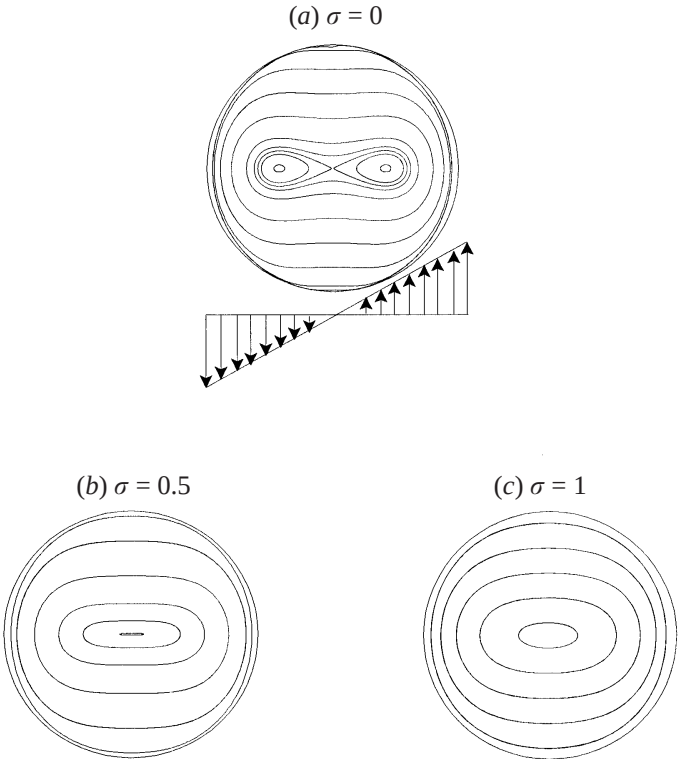

FIGURE 2. Streamlines internal to a neutrally-buoyant droplet suspended within a simple shear flow for various viscosity ratios. The streamlines shown are those lying in the meridian plane containing the simple shearing flow. The remainder of the flow field is similar, but also contains a z-component: $v_z = -xyzG/[2a^2(1+\sigma)]$.

have that $\mathbf{G} = \boldsymbol{i}_1\boldsymbol{i}_2 G$ and $\boldsymbol{\omega} = \boldsymbol{i}_3 G$, with (x_1, x_2, x_3) a system of right-handed rectangular Cartesian coordinates, $(\boldsymbol{i}_1, \boldsymbol{i}_2, \boldsymbol{i}_3)$ the corresponding unit vectors, and G the shear rate. Typical internal streamlines generated by this flow are shown in figure 2. Note that as σ increases, the streamlines approach those for a solid-body rotation. It will be shown later that no chaotic flow exists for these large values of σ.

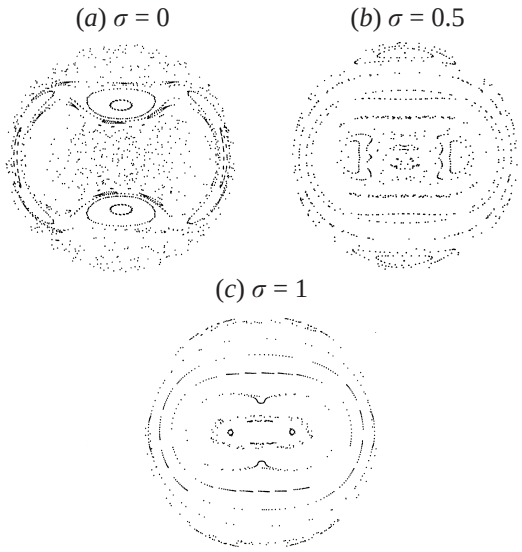

FIGURE 3. Poincaré sections for $\hat{G} = 1$, $\alpha = 0$, and the indicated viscosity ratios.

3. Chaotic trajectories within the drop: Poincaré sections

A qualitative description of the flow may be obtained through the use of Poincaré sections. In the present case we integrate the equation

$$\frac{\mathrm{d}\boldsymbol{x}}{\mathrm{d}t} = \boldsymbol{v}(\boldsymbol{x}) \tag{3.1}$$

governing the Lagrangian trajectories $\boldsymbol{x} \equiv \boldsymbol{x}(\boldsymbol{x}_0, t)$ of the fluid particles, with $\boldsymbol{v}$ the vector velocity field arising from the appropriate superposition of (2.1) and (2.3), and $\boldsymbol{x}$ the position vector at time t of the particular fluid particle whose position vector at time $t = 0$ was $\boldsymbol{x}_0$. Poincaré sections may then be obtained in an appropriately chosen plane, in this case the meridian plane whose unit normal is $\hat{\boldsymbol{g}}$. These plots are similar to those obtained by Stone *et al.* (1991) for more general shear flows.

Three non-dimensional fluid-mechanical parameters arise in the present study: (i) the ratio $\hat{G} \equiv aG/U$, representing the strength of the shear field relative to the bubble rise velocity $U = |\boldsymbol{U}|$; (ii) the internal/external viscosity ratio σ; and (iii) the angle $\alpha = \cos^{-1}(\boldsymbol{i}_3 \cdot \hat{\boldsymbol{g}})$ $(0 \leqslant \alpha \leqslant \frac{1}{2}\pi)$ between the undisturbed vorticity vector and the direction of gravity. (The orientation of the x_1-coordinate is maintained such that throughout this paper the angle $\cos^{-1}(\boldsymbol{i}_1 \cdot \hat{\boldsymbol{g}}) = \frac{1}{2}\pi$.)

Displayed in figure 3 are the Poincaré sections for $\hat{G} = 1$, $\alpha = 0$ (corresponding to a bubble rising perpendicularily to the shear plane) and for varying viscosity ratios σ. These plots were produced using a fourth-order Runga–Kutta method, with a step size small enough that halving it produced the same structure in the Poincaré plots. In most cases the time step was 1×10^{-4} to 1×10^{-5}, the smaller step size being necessary for the more chaotic flows. As is evident, the extent of the chaotic region decreases with increasing σ. Indeed, as $\sigma \to \infty$ the flow becomes completely non-chaotic, with the flow internal to the droplet being simply a rigid-body rotation at angular velocity $\omega/2$

Figure 4 displays Poincaré sections for $\sigma = 0$, $\alpha = 0$ and for several values of $\hat{G}$. For small shear rates, such as $\hat{G} = 0.1$, the particle trajectories are largely quasi-periodic,

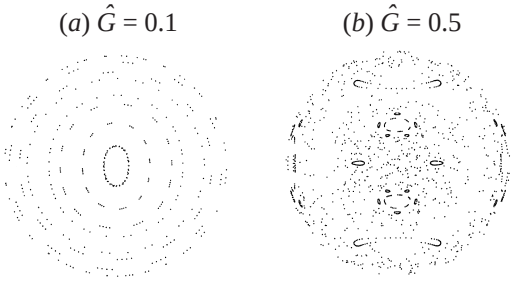

FIGURE 4. Poincaré sections for $\sigma = 0$, $\alpha = 0$, and the indicated shear strength ratios.

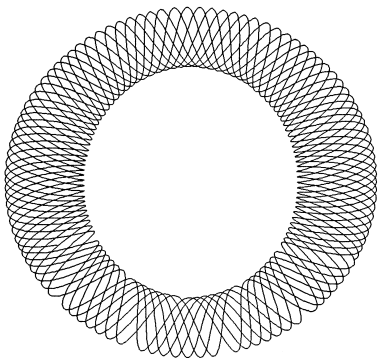

FIGURE 5. Typical trajectory of a particle with $\hat{G} = 0.1$, $\sigma = 0$, and $\alpha = 0$.

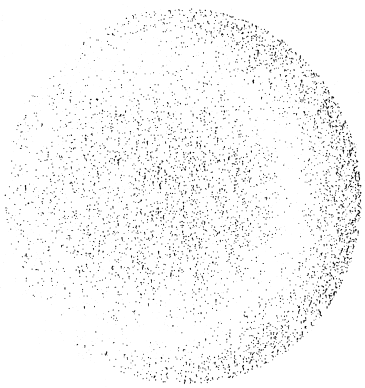

FIGURE 6. Poincaré section for $\sigma = 0$, $\alpha = \pi/4$, and $\hat{G} = 1$.

with particles traversing the surface of a torus (see figure 5). Although extremely small chaotic regions may exist, they were not detectable in these maps and would not be large enough to be of practical importance. Larger values of $\hat{G}$ result in correspondingly larger regions of the flow containing chaotic trajectories.

Figure 6 depicts the Poincaré section resulting when $\hat{G} = 1$, $\sigma = 0$, and $\alpha = \frac{1}{4}\pi$. This flow exhibits considerable chaotic behaviour, with one initial condition sampling apparently all of the droplet. In contrast, for $\alpha = \frac{1}{2}\pi$ the resulting particle trajectories differ qualitatively from those at other angles. Indeed, since the respective internal flows generated by the translation and shear flows lie in the same plane, the resulting particle trajectories are purely periodic.

4. Effective mass-transfer coefficients

This section furnishes a calculation of the rate at which a passive solute, initially dissolved in the droplet and absent from the bulk fluid, is transferred into the latter. The resistance to interphase mass transfer will be assumed governed locally by an external mass-transfer coefficient k which is independent of surface position. (Our analytical and computational methods are equally applicable to circumstances in which the mass-transfer coefficient k, rather than being constant, varies in a prescribed manner over the surface of the droplet, e.g. Lochiel & Calderbank 1964; Baird & Hamielec 1962.) Our goal is to determine the overall rate of interphase mass transfer by investigating the internal convective and diffusive transport processes occurring within the droplet. During the process the external fluid will be assumed to act simply as an infinite reservoir for solute, and hence to remain permanently everywhere at zero local solute concentration throughout the extraction process.

The instantaneous solute concentration $c(\boldsymbol{x}, t)$ within the droplet obeys the standard convective–diffusive equation

$$\frac{\partial c}{\partial t} + \boldsymbol{v} \cdot \nabla c - D\nabla^2 c = 0, \tag{4.1}$$

subject to the respective initial and boundary conditions,

$$c = c_0 \quad \text{at} \quad t = 0, \tag{4.2}$$

$$D\frac{\partial c}{\partial r} = -kc \quad \text{at} \quad r = a, \tag{4.3}$$

where $c_0 \equiv c(\boldsymbol{x}, 0)$ is taken to be a constant. The results ultimately obtained for the overall mass-transfer coefficient K defined in (4.4) are independent of this arbitrary choice of initial solute distribution, the constancy of c_0 being chosen merely for convenience.

These equations were solved numerically using an alternating-direction finite-difference method, and the overall mass-transfer coefficient subsequently calculated as

$$K = -\lim_{t\to\infty} \frac{1}{\Delta t} \ln \left(\frac{\int_V c(\boldsymbol{x}, t + \Delta t) \mathrm{d}V}{\int_V c(\boldsymbol{x}, t) \mathrm{d}V} \right), \tag{4.4}$$

in which Δt is an arbitrarily short time interval and V denotes the droplet domain. This approach is equivalent to solving the generalized Taylor dispersion zeroth-order local moment eigenvalue problem (Brenner & Edwards 1993). (See Edwards, Shapiro & Brenner 1993 for a proof of this equivalence.) This asymptotic mass-transfer coefficient provides a global measure of the effectiveness of the chaotic flow field in enhancing the solute transport processes occurring within the droplet. It has the advantage of being independent of initial conditions, and is comparable in nature to the effective reaction-rate coefficient (Bryden & Brenner 1996) for circumstances wherein the solute is depleted by a first-order irreversible chemical reaction (quantified by a kinetic reaction-rate coefficient k) occurring at the interface. The global physical significance of K lies in the fact that it appears as the coefficient of the exponential decay term in the asymptotic relation

$$M(t) \sim M_f \mathrm{e}^{-Kt} \tag{4.5}$$

governing the mass $M(t) = \int_V c(\boldsymbol{x}, t) \mathrm{d}V$ of solute remaining in the droplet at time t for

times t satisfying the inequality $t \gg a^2/D$, with M_f the fictitious mass of solute initially present (Shapiro & Brenner 1987); that is, $M_f \neq M(0)$, where $M(0) = \int_V c(\boldsymbol{x}, 0)\mathrm{d}V \equiv c_0 V$ in present circumstances. Calculation of M_f is discussed in §5 (see table 1).

For a fixed Sherwood number $Sh = ka/D$, we parametrically explored the effects on K of varying the: (i) translational Péclet number ($Pe = Ua/D$); (ii) shear strength/bubble rise velocity ratio $\hat{G}$; (iii) relative orientation α of the shear and translational flows; and (iv) viscosity ratio σ. Typical Péclet numbers for liquid droplets of diameters 0.1 to 10 mm are of order 10^5 to 10^{10} for hydrocarbon-aqueous systems. Such extremely high Péclet numbers can cause numerical instabilities in the requisite calculations. However, it proved unnecessary to carry out calculations at very large Péclet numbers, since clearly defined trends became evident at much smaller values. Indeed, for many sets of parameters, especially those which give rise to significant regions of regular motions, an asymptotic limit was already achieved at values of $Pe \approx 100$. Asymptotic limits were also observed at large Sherwood numbers.

All the calculations reported here employed a value of $Sh = 100$, just slightly below the asymptotic limit at which the interphase transport rate becomes independent of k. Thus, the results reported herein furnish an approximation to the case wherein the external mass-transfer coefficient becomes infinite, that is, when the boundary condition (4.3) is replaced by the condition $c = 0$ at $r = a$. Interest in the latter boundary condition arises from the fact that, all other things being equal, chaotic mixing effects within the drop are expected to maximally enhance the rate of solute transport into the entraining fluid for circumstances in which the external mass-transfer coefficient k appearing in (4.3) is infinite; for then, solute transport within the droplet interior constitutes the rate-limiting mechanism controlling the interphase transfer rate. Hence, the $k = \infty$ case represents the most interesting case for studying transport enhancement by chaotic advection.

Unfortunately, the $c = 0$ at $r = a$ boundary condition leads to numerical instabilities at large Péclet numbers, the case of interest in applications. Thus, rather than treat this case directly, we did so indirectly by studying the case of large, but finite, Sherwood numbers. This was done by initially parametrically exploring the non-dimensional interphase transport rate Ka^2/D as a function of the Sherwood number until the latter was sufficiently large for the interphase transport rate to be almost maximized, all other things being equal. Investigation revealed that this asymptotic state was approximately achieved at $Sh = 100$, whence we fastened upon this particular value for all of our calculations. This choice allowed us to bring our computations to fruition in a reasonable amount of computer time, even for asymptotically large Péclet numbers.

Figure 7 displays the effective mass-transfer coefficient K as a function of Pe for $\alpha = 0$, $\sigma = 0$, and for various values of $\hat{G}$. With the exception of the $\hat{G} = 0.1$ case, each of these flows possesses chaotic regions (see figures 3(*a*) and 4). Also shown are the mass-transfer coefficients obtained when only one of the two basic flows, shear or translation, is present. For small Péclet numbers the extraction rate approaches that occurring in the absence of flow, namely the smallest root of $\tan\lambda = \lambda/(1 - Sh)$, with $\lambda = Ka^2/D|_{Pe=0}$ (approximately 9.67 for the present value of $Sh = 100$). From these results, it is clear that those flows which are chaotic, (cf. figures 3*a* and 4*b*), result in the largest extraction rates, whereas the quasi-periodic case ($\hat{G} = 0.1$) is nearly indistinguishable from the case of pure translational motion. The extraction rate induced by the shear flow alone is scarcely larger than that for the purely diffusive case. The latter behaviour is expected, since many of the streamlines for this case

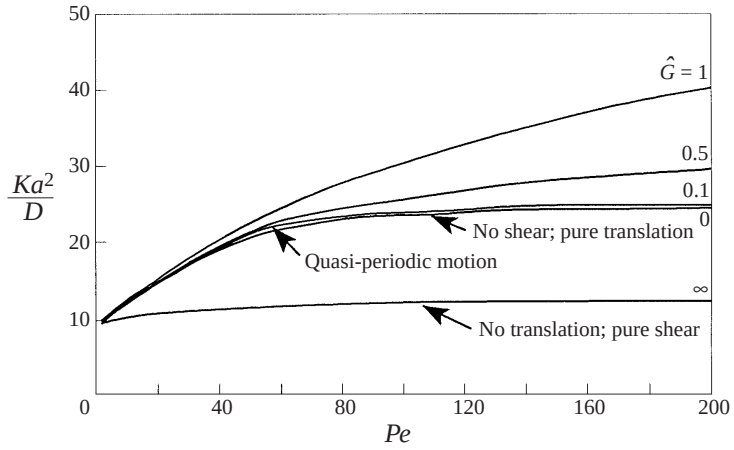

FIGURE 7. Effective mass-transfer coefficient as a function of Péclet number for $\alpha = 0$, $\sigma = 0$, $Sh = 100$, and various values of $\hat{G}$. The value $\hat{G} = \infty$ corresponds to the case of no translation of the droplet. (In this case the value appearing on the abscissa is the shear Péclet number, $Pe_G = a^2\hat{G}/D$. For a given Pe_G the strength of the shear field is identical to that present for $Pe = Pe_G$ and $\hat{G} = 1$.)

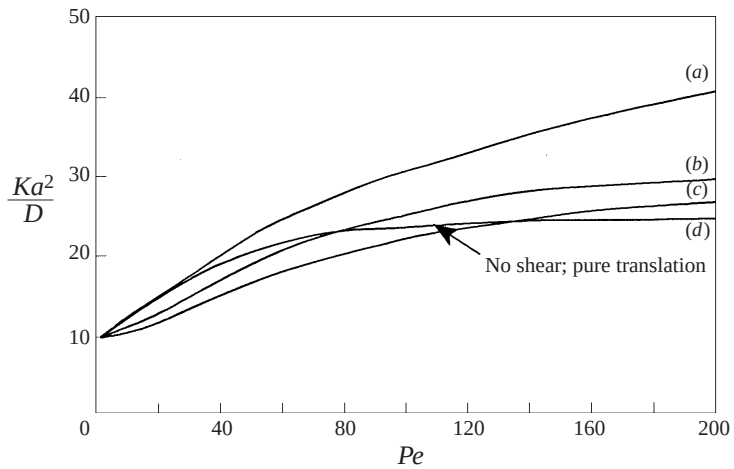

FIGURE 8. Effective mass-transfer coefficient as a function of Péclet number for $\alpha = 0$, $Sh = 100$, and (*a*) $\hat{G} = 1$, $\sigma = 0$; (*b*) $\hat{G} = 1$, $\sigma = 0.5$; (*c*) $\hat{G} = 1$, $\sigma = 1$; (*d*) $\hat{G} = 0$, $\sigma = 0$.

resemble those for solid-body rotation; and a purely rotary internal flow contributes nothing to the transport of solute towards the droplet surface. From a comparison of figures 3(*a*) and 4(*b*) it is not obvious which of the two flows, $\hat{G} = 0.5$ or $\hat{G} = 1$, is the more chaotic in nature, since each Poincaré section contains several regular islands. In contrast with such purely qualitative attempts to distinguish the more chaotically effective of these two flows, the quantitative rate results of figure 7 clearly distinguish between them.

The influence of the viscosity ratio σ on mass transfer is illustrated in figure 8. Again, it is seen that those flows which appear visually to be most chaotic are also those that result in the largest mass-transfer rates.

Figure 9 furnishes the effective extraction rate as a function of Pe (with $\sigma = 0$ and

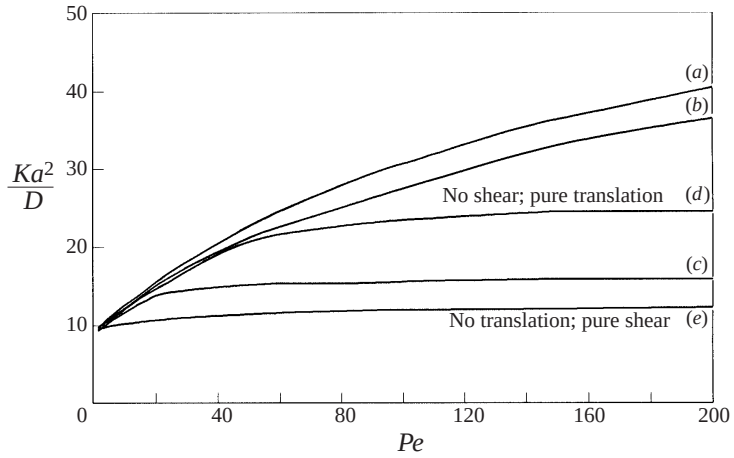

FIGURE 9. Effective mass-transfer coefficient as a function of Péclet number for $\sigma = 0$, $Sh = 100$, and (*a*) $\hat{G} = 1$, $\alpha = 0$; (*b*) $\hat{G} = 1$, $\alpha = \pi/4$; (*c*) $\hat{G} = 1$, $\alpha = \pi/2$; (*d*) $\hat{G} = 0$; (*e*) no translation ($\hat{G} \to \infty$).

$\hat{G} = 1$) for three possible relative orientations α of the directions of gravity and shear, namely (i) $\alpha = 0$ (translational motion parallel to the vorticity vector); (ii) $\alpha = \frac{1}{2}\pi$ (translational motion perpendicular to the vorticity vector); (iii) $\alpha = \frac{1}{4}\pi$. As noted earlier, when $\alpha = \frac{1}{2}\pi$ the trajectories are periodic, whereas in the remaining cases they are largely chaotic. It is clear that the chaotic flows again result in greater extraction rates than those for comparable non-chaotic flows. Indeed, the effective mass-transfer coefficient for the $\alpha = \frac{1}{2}\pi$ case is even less than that occurring in the absence of shear! This result is a consequence of the streamline pattern for this flow. Superposition of translation and shear lying in the same plane results in the disappearance of streamlines that circulate from the centre of the droplet towards the exterior, despite their presence in the case of pure translation. Rather, the streamlines are now closer in configuration to concentric circles, thus contributing little to the extraction rate. Finally, the mass-transfer coefficient is seen to be greater for $\alpha = 0$ than for $\alpha = \frac{1}{4}\pi$ despite the apparently larger extent of chaos visible in the latter case. Thus, while the presence of chaos in these flows enhances the mass-transfer rates relative to those for comparable non-chaotic flows, the extent of the chaos does not always provide an accurate qualitative correlation of the global rate of transport.

5. Discussion

Although only bubbles with inviscid interfaces have been considered, the results obtained herein may nonetheless be applied to circumstances in which the interface is viscous (i.e. possesses its own intrinsic Newtonian interfacial rheological properties), provided that appropriate changes are made in the respective denominators of (2.1) and (2.3), as well as in the magnitude U of the translational velocity. This is a consequence of the fact that the configuration of the streamlines arising from the bubble's translational motion is unaffected by the existence of interfacial viscosity; only the magnitude of U is influenced by the interfacial rheology (Edwards *et al.* 1991). Thus, the velocity field resulting from translational motion occurring in the presence of interfacial rheology is identical to that for an inviscid bubble, with the

σ	$\hat{G}$	α	Ka^2/D	$M_f/M(0)$
0	0	0	24.4	0.83
0	∞	0	12.0	0.60
0	0.1	0	23.5	0.83
0	0.5	0	29.4	0.84
0	1	0	40.6	1.14
0.5	1	0	30.5	0.95
1	1	0	26.5	0.93
0	1	$\frac{1}{4}\pi$	36.7	1.22
0	1	$\frac{1}{2}\pi$	15.8	0.54

TABLE 1. Effective mass-transfer coefficient Ka^2/D and fictitious/true initial solute mass ratio $M_f/M(0)$ for the uniform initial solute concentration case, with $Pe = 200$, $Sh = 100$, and the parametric trio sets cited herein.

quantity $\sigma + \kappa^s/a\mu_o$ (in which κ^s is the surface dilatational viscosity) appearing in place of the viscosity ratio σ in (2.1) and (2.2). Similarly, for small Reynolds and capillary numbers, interfacial rheology affects the droplet velocity field created by the external shear flow only through the denominator appearing on the right-hand side of (2.3) (Edwards *et al.* 1991), in which σ is then replaced by $\hat{\sigma} \overset{\text{def}}{=} \sigma + (5\mu_o a)^{-1}(4\mu^s + 6\kappa^s)$, with μ^s the surface shear viscosity. Furthermore, the value of $\hat{\sigma}$ varies over the range 0 to ∞ for both viscous and inviscid interfaces. Hence, by means of appropriate scaling, the results found here may also be applied to circumstances in which the interface is viscous.

In order to use (4.5) to predict the amount of solute remaining within the droplet at a given time t after the experiment commences, it is necessary to calculate the *fictitious* amount of solute M_f initially present in the droplet at $t = 0$ (Brenner & Edwards 1993). Use of a fictitious initial value in place of the true value corrects for those transport processes occurring prior to the time $t = O(a^2/D)$ at which the present global asymptotic description embodied in (4.5) becomes valid. Calculation of M_f requires determining the solution $A(\boldsymbol{x})$ of the steady-state differential equation

$$\boldsymbol{v} \cdot \nabla A + D\nabla^2 A + KA = 0, \tag{5.1}$$

subject to the respective boundary and normalization conditions

$$D\frac{\partial A}{\partial r} = -kA \quad \text{at} \quad r = a, \tag{5.2}$$

$$\int_V P_0^\infty A \mathrm{d}V = 1, \tag{5.3}$$

in which

$$P_0^\infty(\boldsymbol{x}) = \lim_{t\to\infty}\left\{ c(\boldsymbol{x},t) \Big/ \int_V c(\boldsymbol{x},t)\mathrm{d}V \right\} \tag{5.4}$$

represents the long-time 'non-reactive' zeroth-order local moment (Brenner & Edwards 1993). For a specified true initial solute concentration $c(\boldsymbol{x}, 0)$, the fictitious mass M_f of solute initially present in the droplet is then found through the quadrature

$$M_f = \int_V c(\boldsymbol{x},0)A(\boldsymbol{x})\mathrm{d}V. \tag{5.5}$$

For $Pe = 200$, table 1 displays the ratio of fictitious to true initial solute masses, $M_f/M(0)$, where $M(0) \equiv c_0 V$ is the true mass of solute initially present in the drop for the case described by (4.1) to (4.3). Equivalently, if we define a fictitious (uniform) initial solute concentration c_f as $c_f = M_f/V$, then $M_f/M(0) \equiv c_f/c_0$ represents the ratio of fictitious to true initial homogeneous solute concentration in the droplet.

The problem of extracting a solute from a translating droplet was addressed by Kronig & Brink (1949). They found an approximate solution for asymptotically large Péclet and Sherwood numbers. The asymptotic global extraction-rate coefficient $Ka^2/D = 24.4$ furnished by our calculations in the absence of shear (cf. table 1) agrees quite well with the limiting value of 26.85 found by Kronig & Brink (1949) for the infinite Sherwood number case, the slight difference presumably being due to the difference in Sherwood numbers. However, our fictitious/true initial mass ratio of $M_f/M(0) = 0.83$ is larger than the value of 0.65 quoted by Kronig & Brink (1949). Our calculations showed that this ratio approaches its limiting asymptotic value at much larger values of both Pe and Sh than does K. Additional calculations performed with $Sh = 500$ and $Sh = 800$ (in place of $Sh = 100$) and $Pe = 200$ each provided identical values of 25.8 and 0.69 for the respective values of Ka^2/D and $M_f/M(0)$, whereas a calculation with $Sh = 500$ and $Pe = 300$ provided the respective values of 26.1 and 0.66, suggesting the possibility of excellent agreement between these two very different modes of calculation at $Sh = \infty$, $Pe = \infty$.

6. Conclusions

We have demonstrated that chaotic low Reynolds number flows can arise within a spherical droplet by superposing translational and simple shear flows. Moreover, the presence of chaotic streamlines is shown to significantly increase the rate of extraction of a solute from the interior of the droplet into the bulk fluid, an observation of potential practical importance in the design of mass-transfer devices.

The class of flows studied herein possesses the distinct advantage of being easily realized with elementary equipment. Thus, unique opportunities exist for experimental studies of these chaotic flows. In this context, tracer studies similar to those undertaken for two-dimensional time-dependent chaotic flows (e.g. Swanson & Ottino 1990; Kusch & Ottino 1992; Dutta & Chevray 1995; Saatdjian *et al.* 1996), and three-dimensional, spatially periodic chaotic flows (e.g. Kusch & Ottino 1992), as well as solute extraction experiments, would be expected to usefully supplement the present theoretical analysis. Such realizations would hopefully demonstrate the practical applications of chaotic flows towards improving industrial mass-transfer processes.

The occurrence of chaos in such elementary circumstances as those studied here suggests that other simple, practically relevant, chaotic flows exist, and that they merely await discovery and/or theoretical elucidation before being put to productive use in industrial applications. Indeed, it appears that in many laminar flows, chaos may be the rule rather than the exception.

This work was supported by a National Science Foundation Graduate Fellowship to M.D.B. and by a grant to H.B. from the Office of Basic Energy Sciences of the US Department of Energy.

REFERENCES

Baird, M. H. I. & Hamielic, A. E. 1962 Forced convection transfer around spheres at intermediate Reynolds numbers. *Can. J. Chem. Engng* **10**, 119–121.

Bajer, K. & Moffatt, H. K. 1990 On a class of steady confined Stokes flows with chaotic streamlines. *J. Fluid Mech.* **212**, 337–363.

Brenner, H. & Edwards, D. A. 1993 *Macrotransport Processes.* Butterworth-Heinemann.

Bryden, M. D. & Brenner, H. 1996 Effect of laminar chaos on reaction and dispersion in eccentric annular flow. *J. Fluid Mech.* **325**, 219–237.

Cartwright, J. H. E., Feingold, M. & Piro, O. 1996 Chaotic advection in three-dimensional unsteady incompressible laminar flow. *J. Fluid Mech.* **316**, 259–284.

Dutta, P. & Chevray, R. 1995 Enhancement of mixing by chaotic advection with diffusion. *Exp. Thermal Fluid Sci.* **11**, 1–12.

Edwards, D. A., Brenner, H. & Wasan, D. T. 1991 *Interfacial Transport Processes and Rheology*. Butterworth-Heinemann.

Edwards, D. A., Shapiro, M. & Brenner, H. 1993 Dispersion and reaction in two-dimensional model porous media. *Phys. Fluids* A **5**, 837–858.

Ghosh, S., Chang, H.-C. & Sen, M. 1992 Heat-transfer enhancement due to slender recirculation and chaotic transport between counter-rotating eccentric cylinders. *J. Fluid Mech.* **238**, 119–154.

Hadamard, J. S. 1911 Mouvement permenent lent d'une sphere liquide et visqueuse dans un liquide visqueux. *C. R. Acad. Sci. Paris* **152**, 1735–1738.

Happel, J. & Brenner, H. 1983 *Low Reynolds Number Hydrodynamics.* Kluwer.

Jana, S. C. & Ottino, J. M. 1992 Chaos-enhanced transport in cellular flows. *Phil. Trans. R. Soc. Lond.* A **338**, 519–532.

Kronig, R. & Brink, J. C. 1949–1951 On the theory of extraction from falling droplets. *Appl. Sci. Res.* **A2**, 142–154.

Kusch, H. A. & Ottino, J. M. 1992 Experiments on mixing in continuous chaotic flows. *J. Fluid Mech.* **236**, 319–347.

Lochiel, A. C. & Calderbank, P. H. 1964 Mass transfer in the continuous phase around axisymmetric bodies of revolution. *Chem. Engng Sci.* **19**, 472–484.

Ottino, J. M. 1990 Mixing, chaotic advection, and turbulence. *Ann. Rev. Fluid Mech.* **22**, 207–253.

Saatdjian, E., Midoux, N., Gastou Chassaing, M.I., Leprevost, J. C. & André, J. C. 1996 Chaotic mixing and heat transfer between confocal ellipses: experimental and numerical results. *Phys. Fluids* **8**, 677–691.

Shapiro, M. & Brenner, H. 1987 Chemically reactive generalized Taylor dispersion phenomena. *AIChE J.* **33**, 1155–1167.

Stone, H. A., Nadim, A. & Strogatz, S. 1991 Chaotic streamlines inside drops immersed in steady Stokes flows. *J. Fluid Mech.* **232**, 629–646.

Swanson, P. D. & Ottino, J. M. 1990 A comparative computational and experimental study of chaotic mixing of viscous fluids. *J. Fluid Mech.* **213**, 227–249.

Taylor, G. I. 1932 The viscosity of a fluid containing small drops of another fluid. *Proc. R. Soc. Lond.* A **138**, 41–48.

Toussaint, V., Carrière, P. & Raynal, F. 1995 A numerical Eulerian approach to mixing by chaotic advection. *Phys. Fluids* **7**, 2587–2600.